ANALYSIS OF A NEW NONLINEAR SOLUTION OF RELATIVE ORBITAL MOTION

Mary T. Stringer[(1)], **Brett Newman**[(2)], **T. Alan Lovell**[(3)], **and Ashraf Omran**[(4)]
[(1),(2)]*Old Dominion Univ.,Dept. of Mech. & Aerospace Engr., ECSB 1300, Norfolk, VA 23529, (757) 683-3270, mary.t.stringer1@navy.mil, newman@aero.odu.edu*
[(3)]*Air Force Research Laboratory, 3550 Aberdeen Ave. SE, Kirtland AFB, NM 87117, (505) 853-4132, thomas.lovell@kirtland.af.mil*
[(4)]*CNH-Fiat Industrial, 6900 Veterans Blvd., Burr Ridge, IL 60527, (630) 887-3884, ashraf.omran@cnh.com*

Abstract: *Application of Volterra multi-dimensional convolution theory to the nonlinear J_2 perturbed circular relative motion problem is considered in this paper. A complete analytic second order solution for the three-dimensional time dependent relative motion positions in the unperturbed case is generated. Deputy closed-form response expressions are in terms of linear, quadratic, and bilinear combinations of the initial conditions and the chief orbital elements. The Clohessy-Wiltshire linear solution is found to be embedded within the broader nonlinear solution, and the additional nonlinear terms are used to examine and reveal characteristics of the nonlinear relative motion, including amplification, attenuation, and/or reversal of the in-track drift rate. For the investigated example, accuracy of the second order solution improves significantly on that for the linear solution.*

Keywords: *orbital mechanics, relative motion, spacecraft dynamics, nonlinear dynamics, Volterra series, Carlman linearization.*

1. Introduction

Movement between one or more space objects, when separation distances are a small fraction of positions to the primary gravitational body, is an important branch of orbital mechanics and astrodynamics, and is denoted as relative motion. The reference object, or reference point in space-time, is typically referred to as the "chief", while other objects are referred to as "deputies". Relative motion between a chief and deputy has been utilized significantly since the beginning of human spaceflight in 1961 for rendezvous and docking in the context of mission staging, supply and maintenance, stereoscopic sensing, and synthetic aperture transceiving. The subject continues to receive high attention focused on precision, autonomous, multi-vehicle formation flight and close proximity operations.

Hill was the first analyst to give serious mathematics based study to this subject in the context of three-body lunar-geo relative motion [1]. A state transition matrix analytic solution to the linear circular chief relative motion problem based on rectangular coordinates was offered by Clohessy and Wiltshire [2] to solve the rendezvous boundary value problem. This work has been the foundation for a large majority of relative motion research and in-flight applications. Lawden [3] and Tschauner and Hempel [4] extended this analysis and derived analytic solutions to the linear elliptic chief case. Additional solutions have been presented by Carter [5,6] and Yamanaka and Ankersen [7]. Part of the motivation for these authors' solutions has been the presence of singularities in the Tschauner-Hempel solution and the search for more convenient, compact forms for the solution. Inalhan, Tillerson, and How [8] explored the elliptic case state transition solution for periodic formation flight constellations. Hablani, Tapper, and Dana-Bashian [9] studied a multi-pulse exponential glideslope strategy for circular relative motion operations, and Okasha and Newman [10] extended this concept to the elliptic case. Nearly all of this work is based on linear unperturbed model assumptions.

In recent years, efforts have been directed to higher fidelity modeling by incorporating nonlinear and/or perturbation aspects. Schweighart and Sedwick [11] introduced an approximate linear J_2 perturbed model for relative motion with circular chief. The oblate accelerative term is linearized in an ad hoc manner, and is time averaged to obtain a constant coefficient model. Ross [12] provides a more rigorous framework for model development but ignores perturbations to chief mean motion and angular rate. Sengupta, Vadali, and Alfriend [13] offer a model including the short period variations of the mean nonsingular orbital elements. Gim and Alfriend [14] have developed an analytic state transition solution for the J_2 perturbed elliptic chief case including short period and long period effects. Vadali [15] also derived a model and analyzed its accuracy for a mean circular chief accounting for secular drift rates and short period variations in the chief element evolutions. Vaddi, Vadali, and Alfriend [16] used a direct perturbation technique to derive two different analytic expressions for relative motion, first with an elliptic chief, and second with quadratic gravitational acceleration terms, and combined the results for an overall solution. All of these advancements provide engineering utility. Condurache and Martinusi [17,18] have recently offered two exact closed-form solutions to the unperturbed but nonlinear relative motion problem. One solution is based on tensor-vector regularization theory, while the other uses quaternion algebra theory. Impact from these new results is unclear at this time.

In this paper, application of Volterra multi-dimensional convolution theory is applied to the nonlinear J_2 perturbed circular relative motion problem. Approximate analytic expressions for the time dependent deputy positions in terms of initial conditions, chief elements, and gravity parameters are obtained, although unperturbed results are emphasized here. The Clohessy-Wiltshire (CW) linear solution is found to be embedded within the broader nonlinear solution, and the additional nonlinear terms are used to examine characteristics of the associated motion. Further, accuracy of the nonlinear solution improves significantly on that for the linear solution. The work here greatly expands on that provided in the preliminary investigation of Ref. [19]. Section 2 presents the basic ideas behind Volterra theory and how the integral kernels can be estimated by Carleman linearization theory. Section 3 covers the dynamic modeling of relative orbital motion including expansion of the gravitational term through second order for a circular chief and J_2 perturbation. Section 4 maps the dynamic model to the proper Volterra-Carleman form, and the nonlinear unperturbed analytic response expressions are generated. Section 5 demonstrates the fidelity of the new solution in a numeric example. Section 6 then uses the analytic solution to reveal insights into nonlinear relative orbital motion.

2. Volterra Multi-Dimensional Convolution Theory

Many physical systems can be described by a set of nonlinear differential and algebraic equations involving state, input, and output variables. A common representation is the nonlinear state space form, or

$$\begin{aligned} \dot{x}(t) &= f\{x(t),u(t)\} \\ y(t) &= g\{x(t),u(t)\} \end{aligned} \tag{1}$$

where $x \in \mathcal{R}^n$ denotes the state vector, $u \in \mathcal{R}^q$ the input vector, and $y \in \mathcal{R}^p$ the output vector. Vectors $f \in \mathcal{R}^n$ and $g \in \mathcal{R}^p$ denote the system nonlinearities and $t \in \mathcal{R}^1$ is time. Some nonlinear systems are exactly solvable; many others, which are not analytically tractable, can be solved by numerical integration. Although numerical techniques provide high accuracy results, analytic solutions are still sought in order to interpret the physical meaning underneath a solution. The Volterra series [20,21] is one such approach, which can represent a wide range of nonlinear system behavior. The theory represents the input-output relation of a nonlinear system as an infinite sum of multi-dimensional convolution integrals. Thus, the solution of Eq. (1) is represented as

$$y(t) = h_0(t) + \sum_{k=1}^{\infty} \int_0^{\infty}\int_0^{\infty} \cdots \int_0^{\infty} h_k(\tau_1,\tau_2,\ldots,\tau_k) \prod_{i=1}^{k} u(t - \tau_i) d\tau_i \qquad (2)$$

In Eq. (2), $h_k(\tau_1,\tau_2,\ldots,\tau_k)$ denotes the k^{th} order Volterra kernel. Volterra kernels are causal symmetric functions with respect to their argument. Kernel $h_0(t)$ represents the response of the output due to the initial system state, but which also depends indirectly on the input. If the system motion is started at an equilibrium condition (both state and input values) and the equilibrium input is maintained, the $h_0(t)$ kernel equals zero. On the other hand, if the state value is mismatched to the equilibrium input, or vice versa, the $h_0(t)$ kernel is nonzero and can be interpreted as motion of the system from the initial state to the equilibrium state (stable), or the state reacting to the input. All other kernels represent the behavior of the system in response to arbitrary input. These Volterra kernels are combined with the inputs in a multi-dimensional convolution integration. Kernels are a signature of the system characteristics and are unique for a given system. For weak nonlinearities, all higher-order kernels are seen to quickly tend to negligible values, and for a completely linear system, only $h_0(t)$ and $h_1(\tau_1,\tau_2)$ remain.

Since kernels are the backbone of Volterra theory, they must be constructed by some means. Several methodologies are available to estimate the Volterra kernels. Carleman linearization or bilinearization is a useful technique for this purpose and has the ability to deliver an approximate but general analytical solution for the kernels. This method is considered for the relative motion problem. The general outline of the method for a scalar input is first presented to show the mechanism by which the analytical kernels can be constructed.

The single-input multiple-output state space representation of the nonlinear affine system is defined as

$$\begin{aligned} \dot{x}(t) &= F\{x(t)\} + G\{x(t)\}\, u(t) \\ y(t) &= H\{x(t)\} \end{aligned} \qquad (3)$$

where $x \in \mathcal{R}^n$, $u \in \mathcal{R}^1$, $y \in \mathcal{R}^p$, $F \in \mathcal{R}^n$, $G \in \mathcal{R}^n$, $H \in \mathcal{R}^p$, $t \in \mathcal{R}^1$. Carleman linearization is applied to $F\{x(t)\}$, $G\{x(t)\}$, $H\{x(t)\}$ as

$$\begin{aligned} F\{x(t)\} &= A_1(t)x^{(1)}(t) + A_2(t)x^{(2)}(t) + \ldots + A_i(t)x^{(i)}(t) + \ldots \\ G\{x(t)\} &= B_0(t) + B_1(t)x^{(1)}(t) + B_2(t)x^{(2)}(t) + \ldots + B_i(t)x^{(i)}(t) + \ldots \\ H\{x(t)\} &= C_1(t)x^{(1)}(t) + C_2(t)x^{(2)}(t) + \ldots + C_i(t)x^{(i)}(t) + \ldots \end{aligned} \qquad (4)$$

where

$$x^{(0)} = 1 \quad , \quad x^{(1)} = x \quad , \quad x^{(2)} = x \otimes x \quad , \quad x^{(3)} = x \otimes x \otimes x \quad , \ldots , \quad x^{(i)} = x \prod_{k=1}^{i-1} \otimes x \qquad (5)$$

In Eq. (5), $\otimes$ is the Kronecker product defined in Refs. [19,21]. After retaining only N terms, the approximation to Eq. (3) is

$$\begin{aligned} \dot{x}(t) &\approx \sum_{k=1}^{N} A_k(t)x^{(k)}(t) + \sum_{k=0}^{N-1} B_k(t)x^{(k)}(t)u(t) \\ y(t) &\approx \sum_{k=1}^{N} C_k(t)x^{(k)}(t) \end{aligned} \tag{6}$$

The system in Eq. (6) can be formulated as a bilinear system by deriving the differential equation of $x^{(i)}(t)$ as

$$\begin{aligned} \dot{x}^{(i)}(t) &= \sum_{k=i}^{N} A_{ik}(t)x^{(k)}(t) + \sum_{k=i-1}^{N-1} B_{ik}(t)x^{(k)}(t)u(t) \\ y(t) &= \sum_{k=1}^{N} C_k(t)x^{(k)}(t) \end{aligned} \tag{7}$$

where the coefficient matrices are Kronecker combinations of the original expansion matrices.

$$\begin{aligned} A_{ik}(t) &= A_{k-i+1}(t)\left\{\prod_{j=1}^{i-1}\otimes I_n\right\} + I_n \otimes A_{k-i+1}(t)\left\{\prod_{j=1}^{i-2}\otimes I_n\right\} + \ \dots \ + \left\{\prod_{j=1}^{i-1} I_n \otimes\right\}A_{k-i+1}(t) \\ &\text{for } k = i, i+1, i+2, \ \dots \ , N \quad \text{and} \quad i \geq 2 \quad \text{where Eqs. (6)-(7) define the } i = 1 \text{ case} \\ B_{ik}(t) &= B_{k-i+1}(t)\left\{\prod_{j=1}^{i-1}\otimes I_n\right\} + I_n \otimes B_{k-i+1}(t)\left\{\prod_{j=1}^{i-2}\otimes I_n\right\} + \ \dots \ + \left\{\prod_{j=1}^{i-1} I_n \otimes\right\}B_{k-i+1}(t) \\ &\text{for } k = i-1, i, i+1, \ \dots \ , N-1 \quad \text{and} \quad i \geq 2 \quad \text{where Eqs. (6)-(7) define the } i = 1 \text{ case} \end{aligned} \tag{8}$$

The derivation of Eq. (8) is a sequential one. For example, derivation of $x^{(2)}(t)$ is shown below.

$$\begin{aligned} \frac{d}{dt}[x^{(2)}(t)] &= \frac{d}{dt}[x^{(1)}(t) \otimes x^{(1)}(t)] = \dot{x}^{(1)}(t) \otimes x^{(1)}(t) + x^{(1)}(t) \otimes \dot{x}^{(1)}(t) \\ \frac{d}{dt}[x^{(2)}(t)] &= \{\sum_{k=1}^{N-1} A_k(t)x^{(k)}(t) + \sum_{k=0}^{N-2} B_k(t)x^{(k)}(t)u(t)\} \otimes x^{(1)}(t) \\ &\quad + x^{(1)}(t) \otimes \{\sum_{k=1}^{N-1} A_k(t)x^{(k)}(t) + \sum_{k=0}^{N-2} B_k(t)x^{(k)}(t)u(t)\} \\ \frac{d}{dt}[x^{(2)}(t)] &= \sum_{k=1}^{N-1}[A_k(t) \otimes I_n + I_n \otimes A_k(t)]x^{(k+1)}(t) \\ &\quad + \sum_{k=0}^{N-2}[B_k(t) \otimes I_n + I_n \otimes B_k(t)]x^{(k+1)}(t)u(t) \\ \frac{d}{dt}[x^{(2)}(t)] &\approx \sum_{\tilde{k}=2}^{N} A_{2\tilde{k}}(t)x^{(\tilde{k})}(t) + \sum_{\tilde{k}=1}^{N-1} B_{2\tilde{k}}(t)x^{(\tilde{k})}(t)u(t) \quad \text{where} \quad \tilde{k} = k+1 \end{aligned} \tag{9}$$

Differential equations for $x^{(i)}(t)$ for $i = 1,2,\dots,N$ form the overall bilinear state space model as

$$\begin{aligned} \dot{x}^{\otimes}(t) &= \overline{A}(t)x^{\otimes}(t) + \overline{B}_0(t)u(t) + \overline{B}_1(t)x^{\otimes}(t)u(t) \\ y(t) &= \overline{C}(t)x^{\otimes}(t) \end{aligned} \tag{10}$$

with

$$x^{\otimes}(t) = \begin{bmatrix} x^{(1)}(t) \\ x^{(2)}(t) \\ x^{(3)}(t) \\ \cdots \\ x^{(N)}(t) \end{bmatrix} \quad , \quad \overline{A}(t) = \begin{bmatrix} A_{11}(t) & A_{12}(t) & \dots & A_{1N}(t) \\ 0 & A_{22}(t) & \dots & A_{2N}(t) \\ 0 & 0 & \dots & A_{3N}(t) \\ \cdots & & & \\ 0 & 0 & \dots & A_{NN}(t) \end{bmatrix} \tag{11}$$

$$\bar{B}_0(t) = \begin{bmatrix} B_{10}(t) \\ 0 \\ 0 \\ \cdots \\ 0 \end{bmatrix} \quad , \quad \bar{B}_1(t) = \begin{bmatrix} B_{11}(t) & B_{12}(t) & \ldots & B_{1(N-1)}(t) & 0 \\ B_{21}(t) & B_{22}(t) & \ldots & B_{2(N-1)}(t) & 0 \\ 0 & B_{32}(t) & \ldots & B_{3(N-1)}(t) & 0 \\ \cdots & & & & \\ 0 & 0 & \ldots & B_{N(N-1)}(t) & 0 \end{bmatrix}$$

$$\bar{C}(t) = \left[C_1(t) \;\; C_2(t) \; \ldots \; C_N(t) \right]$$

Finally, closed-form expressions for the Volterra kernels are defined as

$$\begin{aligned} h_0(t_1) &= \bar{C}(t_1)\bar{\Phi}(t_1,0)x_0^{\otimes} \\ h_1(t_1,t_2) &= \bar{C}(t_1)\bar{\Phi}(t_1,t_2)\,\{\bar{B}_0(t_2) + \bar{B}_1(t_2)\bar{\Phi}(t_2,0)x_0^{\otimes}\} \\ h_2(t_1,t_2,t_3) &= \bar{C}(t_1)\bar{\Phi}(t_1,t_2)\bar{B}_1(t_2)\bar{\Phi}(t_2,t_3)\,\{\bar{B}_0(t_3) + \bar{B}_1(t_3)\bar{\Phi}(t_3,0)x_0^{\otimes}\} \\ &\cdots \\ \text{where } \; \bar{\Phi}(t,0) &= e^{\int_0^t \bar{A}(\tau)d\tau} \end{aligned} \tag{12}$$

3. Relative Motion Dynamics

Figure 1 describes the relative motion of a deputy satellite with respect to a chief satellite. Two reference frames are shown. The first frame is the standard XYZ Earth-centered inertial (ECI) frame. The second frame is the xyz local-vertical local-horizontal (LVLH) frame with origin located on the chief, x axis in the radial direction, y axis in the transverse (in-track) direction, and z axis in the normal (cross-track) direction. Chief and deputy absolute position vectors in algebraic form are denoted by $\mathbf{R_c}$ and $\mathbf{R_d}$ while the relative position vector of deputy with respect to chief is $\mathbf{r}$. Position vector components expressed in the LVLH frame are

$$\begin{aligned} \mathbf{R_c} &= [R_c \;\; 0 \; 0]^T \\ \mathbf{R_d} &= \mathbf{R_c} + \mathbf{r} = [(R_c + x) \;\; y \; z]^T \end{aligned} \tag{13}$$

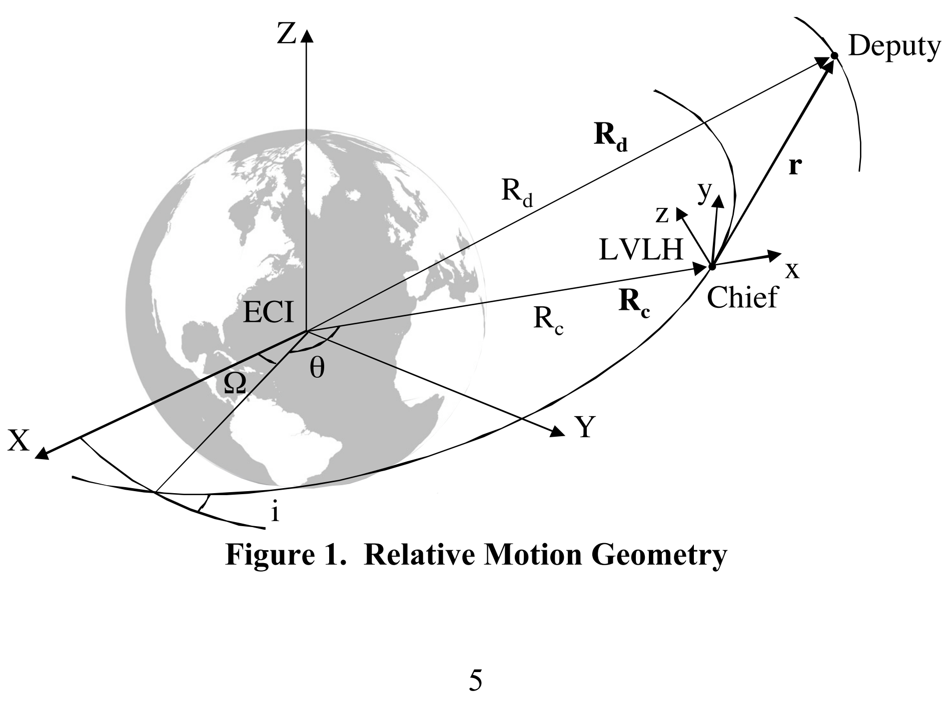

Figure 1. Relative Motion Geometry

Using a relative motion description, and assuming an ideal two-body (J_0) plus oblate (J_2) gravitational field, the governing nonlinear motion equation in algebraic form is

$$\ddot{\mathbf{r}} = -\dot{\Omega}\mathbf{r} - 2\Omega\dot{\mathbf{r}} - \Omega\Omega\mathbf{r} + \nabla\Phi_{J0} + \nabla\Phi_{J2}$$

$$\text{where} \quad \omega = [\omega_x \ \omega_y \ \omega_z]^T \quad , \quad \Omega = \begin{bmatrix} 0 & -\omega_z & \omega_y \\ \omega_z & 0 & -\omega_x \\ -\omega_y & \omega_x & 0 \end{bmatrix} \tag{14}$$

where ω is the LVLH frame angular velocity with respect to the ECI frame. The first three kinematic acceleration terms, which are linear in $\mathbf{r}$ and $\dot{\mathbf{r}}$, can be represented by vector $\mathbf{a_K}$ where

$$\mathbf{a_K} = \left[\tilde{A}_{Kr} \ \tilde{A}_{K\dot{r}}\right]\begin{bmatrix}\mathbf{r} \\ \dot{\mathbf{r}}\end{bmatrix}$$

$$\text{where} \quad \tilde{A}_{Kr} = \begin{bmatrix} \omega_y^2+\omega_z^2 & \dot{\omega}_z-\omega_x\omega_y & -\dot{\omega}_y-\omega_x\omega_z \\ -\dot{\omega}_z-\omega_y\omega_x & \omega_z^2+\omega_x^2 & \dot{\omega}_x-\omega_y\omega_z \\ \dot{\omega}_y-\omega_z\omega_x & -\dot{\omega}_x-\omega_z\omega_y & \omega_x^2+\omega_y^2 \end{bmatrix} \quad , \quad \tilde{A}_{K\dot{r}} = 2\begin{bmatrix} 0 & \omega_z & -\omega_y \\ -\omega_z & 0 & \omega_x \\ \omega_y & -\omega_x & 0 \end{bmatrix} \tag{15}$$

A new model for LVLH frame angular velocity [15] with circular chief and J_2 perturbation is

$$\begin{aligned} \omega_x &= 2\dot{\bar{\Omega}}_o S_{\bar{i}_o} S_{\bar{\theta}_o} \\ \omega_y &= 0 \\ \omega_z &= \dot{\bar{\Omega}}_o C_{\bar{i}_o} + \dot{\bar{\theta}}_o + \frac{1}{4}J_2 n_o\left(\frac{R_E}{\bar{R}_o}\right)^2 C_{2\bar{\theta}_o} S^2_{\bar{i}_o} \end{aligned} \tag{16}$$

where

$$\begin{aligned} \dot{\bar{\Omega}}_o &= -\frac{3}{2}J_2 n_o\left(\frac{R_E}{\bar{R}_o}\right)^2 C_{\bar{i}_o} \quad &, \quad \bar{\theta}_o &= \bar{\theta}_{o_0} + \dot{\bar{\theta}}_o t \\ \dot{\bar{\theta}}_o &= n_o - \frac{3}{2}J_2 n_o\left(\frac{R_E}{\bar{R}_o}\right)^2 (1 - 4C^2_{\bar{i}_o}) \quad &, \quad n_o &= \left(\frac{\mu}{\bar{R}_o^3}\right)^{1/2} \end{aligned} \tag{17}$$

This approximation includes both secular and short period (2θ) effects on the chief elements including radius $R = R_c$, inclination i, argument latitude θ, and ascending node right ascension Ω. Bar and subscript notation refers to mean osculating elements [15] and $S_{"} = \sin(")$, $C_{"} = \cos(")$. Additional variables in Eq. (17) include gravitational parameter μ, Earth radius R_E, and mean motion n_o. After substitution of this model assumption, Eq. (15) can be rearranged as

$$\mathbf{a_K} = \left[A_{Kr} \ A_{K\dot{r}}\right]\begin{bmatrix}\mathbf{r} \\ \dot{\mathbf{r}}\end{bmatrix} + \left[B_{Kr} \ B_{K\dot{r}}\right]\begin{bmatrix}\mathbf{r} \\ \dot{\mathbf{r}}\end{bmatrix} J_2 + \ldots$$

$$\text{where} \quad A_{Kr} = n_o^2\begin{bmatrix} 1 & 0 & 0 \\ 0 & 1 & 0 \\ 0 & 0 & 0 \end{bmatrix} \quad , \quad A_{K\dot{r}} = 2n_o\begin{bmatrix} 0 & 1 & 0 \\ -1 & 0 & 0 \\ 0 & 0 & 0 \end{bmatrix} \tag{18}$$

$$B_{Kr} = \frac{1}{2}n_o^2\left(\frac{R_E}{\bar{R}_o}\right)^2\begin{bmatrix} -a & -b & 3c \\ b & -a & -3d \\ 3c & 3d & 0 \end{bmatrix} \quad , \quad B_{K\dot{r}} = \frac{1}{2}n_o\left(\frac{R_E}{\bar{R}_o}\right)^2\begin{bmatrix} 0 & -a & 0 \\ a & 0 & -6c \\ 0 & 6c & 0 \end{bmatrix}$$

$$a = 6(1 - 3C^2_{\bar{i}_o}) - S^2_{\bar{i}_o} C_{2\bar{\theta}_o} \quad , \quad b = S^2_{\bar{i}_o} S_{2\bar{\theta}_o} \quad , \quad c = S_{2\bar{i}_o} S_{\bar{\theta}_o} \quad , \quad d = S_{2\bar{i}_o} C_{\bar{\theta}_o}$$

Note the bilinear structure of Eq. (18), with J_2 interpreted as an input, is similar to Eq. (7).

The last two terms from Eq. (14) are gradients of the two-body and oblate gravitational potential functions. These terms are nonlinear in **r** and are represented by vectors $\mathbf{a_{J0}}$ and $\mathbf{a_{J2}}$ where

$$\mathbf{a_{J0}} = -\frac{\mu}{R_d^3}\begin{bmatrix} R_c+x \\ y \\ z \end{bmatrix} + \frac{\mu}{R_c^3}\begin{bmatrix} R_c \\ 0 \\ 0 \end{bmatrix}$$

$$\mathbf{a_{J2}} = \frac{3}{2}\frac{\mu}{R_d^3}J_2\left(\frac{R_E}{R_d}\right)^2\begin{bmatrix} (5f^2-1)(R_c+x) - 2fS_iS_\theta R_d \\ (5f^2-1)y \quad - 2fS_iC_\theta R_d \\ (5f^2-1)z \quad - 2fC_iR_d \end{bmatrix} - \frac{3}{2}\frac{\mu}{R_c^3}J_2\left(\frac{R_E}{R_c}\right)^2\begin{bmatrix} (5S_i^2S_\theta^2-1)R_c - 2S_i^2S_\theta^2R_c \\ - 2S_i^2S_\theta C_\theta R_c \\ - 2S_iC_iS_\theta R_c \end{bmatrix} \quad (19)$$

$$\text{where} \quad R_d = \{(R_c+x)^2+y^2+z^2\}^{1/2} \quad , \quad f = S_iS_\theta\frac{R_c+x}{R_d} + S_iC_\theta\frac{y}{R_d} + C_i\frac{z}{R_d}$$

The gravitational nonlinearity in Eq. (19) is approximated through second order using Taylor's expansion about the chief's position with the mean osculating elements.

$$\mathbf{a_{J0}} = \begin{bmatrix} \nabla a_{J0x} \\ \nabla a_{J0y} \\ \nabla a_{J0z} \end{bmatrix}_{\mathbf{r}=\mathbf{0}} \mathbf{r} + \frac{1}{2}\begin{bmatrix} \mathbf{r}^T & 0_{1\times3} & 0_{1\times3} \\ 0_{1\times3} & \mathbf{r}^T & 0_{1\times3} \\ 0_{1\times3} & 0_{1\times3} & \mathbf{r}^T \end{bmatrix}\begin{bmatrix} \nabla(\nabla a_{J0x})^T \\ \nabla(\nabla a_{J0y})^T \\ \nabla(\nabla a_{J0z})^T \end{bmatrix}_{\substack{\mathbf{r}=\mathbf{0}\ ,\ R=\bar{R}_o \\ i=\bar{i}_o\ ,\ \theta=\bar{\theta}_o}} \mathbf{r} + \ldots$$

$$\mathbf{a_{J2}} = \begin{bmatrix} \nabla a_{J2x} \\ \nabla a_{J2y} \\ \nabla a_{J2z} \end{bmatrix}_{\mathbf{r}=\mathbf{0}} \mathbf{r} + \frac{1}{2}\begin{bmatrix} \mathbf{r}^T & 0_{1\times3} & 0_{1\times3} \\ 0_{1\times3} & \mathbf{r}^T & 0_{1\times3} \\ 0_{1\times3} & 0_{1\times3} & \mathbf{r}^T \end{bmatrix}\begin{bmatrix} \nabla(\nabla a_{J2x})^T \\ \nabla(\nabla a_{J2y})^T \\ \nabla(\nabla a_{J2z})^T \end{bmatrix}_{\substack{\mathbf{r}=\mathbf{0}\ ,\ R=\bar{R}_o \\ i=\bar{i}_o\ ,\ \theta=\bar{\theta}_o}} \mathbf{r} + \ldots \quad (20)$$

Equation (20) can be written more conveniently using the Kronecker product.

$$\mathbf{a_{J0}} = A_{J0}\mathbf{r} + A_{J0}^{(2,r)}\mathbf{r^{(2)}} + \ldots$$

$$\mathbf{a_{J2}} = B_{J2}\mathbf{r}J_2 + B_{J2}^{(2,r)}\mathbf{r^{(2)}}J_2 + \ldots$$

$$\text{where} \quad \mathbf{r^{(2)}} = [xx\ xy\ xz\ yx\ yy\ yz\ zx\ zy\ zz]^T$$

$$A_{J0} = n_o^2\begin{bmatrix} 2 & 0 & 0 \\ 0 & -1 & 0 \\ 0 & 0 & -1 \end{bmatrix} \quad , \quad A_{J0}^{(2,r)} = \frac{3}{2}\frac{n_o^2}{\bar{R}_o}\left[\begin{array}{ccc|ccc|ccc} -2 & 0 & 0 & 0 & 1 & 0 & 0 & 0 & 1 \\ 0 & 1 & 0 & 1 & 0 & 0 & 0 & 0 & 0 \\ 0 & 0 & 1 & 0 & 0 & 0 & 1 & 0 & 0 \end{array}\right] \quad (21)$$

$$B_{J2} = \frac{3}{2}n_o^2\left(\frac{R_E}{\bar{R}_o}\right)^2\begin{bmatrix} -4e & 4b & 4c \\ 4b & f & -d \\ 4c & -d & g \end{bmatrix} \quad , \quad B_{J2}^{(2,r)} = \frac{15}{4}\frac{n_o^2}{\bar{R}_o}\left(\frac{R_E}{\bar{R}_o}\right)^2\left[\begin{array}{ccc|ccc|ccc} 4e & -4b & -4c & -4b & -f & d & -4c & d & -g \\ -4b & -f & d & -f & 3b & c & d & c & b \\ -4c & d & -g & d & c & b & -g & b & 3c \end{array}\right]$$

$$e = 3S_{i_o}^2S_{\theta_o}^2 - 1 \quad , \quad f = 5S_{i_o}^2S_{\theta_o}^2 - 1 - 2S_{i_o}^2C_{\theta_o}^2 \quad , \quad g = 5S_{i_o}^2S_{\theta_o}^2 - 1 - 2C_{i_o}^2$$

After collecting all acceleration components, Eq. (14) yields

$$
\begin{aligned}
\ddot{\mathbf{r}} &= \mathbf{a}_{\mathbf{K}} + \mathbf{a}_{\mathbf{J0}} + \mathbf{a}_{\mathbf{J2}} \\
&= \left[(A_{Kr}+A_{J0})\ A_{K\dot{r}}\right]\begin{bmatrix}\mathbf{r}\\ \dot{\mathbf{r}}\end{bmatrix} + A_{J0}^{(2,r)}\mathbf{r}^{(\mathbf{2})} + \ldots \\
&+ \left[(B_{Kr}+B_{J2})\ B_{K\dot{r}}\right]\begin{bmatrix}\mathbf{r}\\ \dot{\mathbf{r}}\end{bmatrix}J_2 + B_{J2}^{(2,r)}\mathbf{r}^{(\mathbf{2})}J_2 + \ldots
\end{aligned}
\tag{22}
$$

Equation (22) is a specific case of the general bilinear model expression in Eq. (7).

4. Second Order Analytic Solution

Coordinates in Eq. (22) require expansion to the full order Kronecker state vector to be consistent with the Carleman linearization process used to obtain the kernels associated with the Volterra multi-dimensional convolution theory. The expansion process is outlined in Eq. (23).

$$
\begin{array}{l}
\begin{bmatrix}\mathbf{r}\\ \dot{\mathbf{r}}\end{bmatrix} \rightarrow x^{(1)} \\
\mathbf{r}^{(\mathbf{2})} \rightarrow x^{(2)}
\end{array}
\quad \text{where} \quad
\begin{array}{l}
x^{(1)} = \left[x\ y\ z\ \dot{x}\ \dot{y}\ \dot{z}\right]^T \\
x^{(2)} = \left[xx\ \ xy\ \ xz\ \ x\dot{x}\ \ x\dot{y}\ \ x\dot{z} \quad yx\ \ yy\ \ yz\ \ y\dot{x}\ \ y\dot{y}\ \ y\dot{z} \quad \ldots \quad \dot{z}\dot{z}\right]^T
\end{array}
\tag{23}
$$

With this step, the motion equation in Eq. (22) becomes

$$
\begin{gathered}
\dot{x}^{(1)} = A_1 x^{(1)} + A_2 x^{(2)} + B_1 x^{(1)} J_2 + B_2 x^{(2)} J_2 \\
A_1 = \begin{bmatrix} 0_3 & I_3 \\ A_{Kr}+A_{J0} & A_{K\dot{r}} \end{bmatrix},\ A_2 = \begin{bmatrix} 0_{3\times36} \\ A_{J0}^{(2)} \end{bmatrix},\ B_1 = \begin{bmatrix} 0_3 & 0_3 \\ B_{Kr}+B_{J2} & B_{K\dot{r}} \end{bmatrix},\ B_2 = \begin{bmatrix} 0_{3\times36} \\ B_{J2}^{(2)} \end{bmatrix}
\end{gathered}
\tag{24}
$$

After generating the second order governing equation, the overall Carleman bilinear model is

$$
\begin{bmatrix}\dot{x}^{(1)}\\ \dot{x}^{(2)}\end{bmatrix} = \begin{bmatrix} A_{11} & A_{12} \\ 0_{36\times6} & A_{22}\end{bmatrix}\begin{bmatrix}x^{(1)}\\ x^{(2)}\end{bmatrix} + \begin{bmatrix} B_{11} & 0_{6\times36} \\ B_{21} & 0_{36}\end{bmatrix}\begin{bmatrix}x^{(1)}\\ x^{(2)}\end{bmatrix}J_2
\tag{25}
$$

or in compact form the model becomes

$$
\begin{aligned}
\dot{x}^{\otimes}(t) &= \overline{A}(t)x^{\otimes}(t) + \overline{B}_0(t)u(t) + \overline{B}_1(t)x^{\otimes}(t)u(t) \\
y(t) &= \overline{C}(t)x^{\otimes}(t)
\end{aligned}
\tag{26}
$$

The dynamical model in Eq. (25) can be utilized for generating closed-form Volterra kernel expressions, which are suitable for the multi-dimensional convolution based analytic solution to the nonlinear J_2 perturbed circular relative motion problem, in terms of initial conditions, chief elements, and gravity parameters. However, the remaining portion of this paper emphasizes only the unperturbed solution. In this case, the bilinear state space model becomes unforced, being excited only by initial conditions. After neglecting the oblate gravitational terms ($u = J_2 = 0$), matrix $\overline{A}$ is the only matrix of significance in the system. Matrix $\overline{C}$ consists of identity and zero matrices to yield deputy x, y, z relative positions as system outputs. Matrix $\overline{A}$, which has dimension 42×42, is defined below.

$$\bar{A} = \left[\begin{array}{c|c} A_{11} & A_{12} \\ \hline 0_{36\times 6} & A_{22} \end{array}\right] = \left[\begin{array}{c|ccc|ccc} A_1 & M_1 & M_2 & M_3 & 0_6 & 0_6 & 0_6 \\ \hline 0_6 & A_1 & 0_6 & 0_6 & I_6 & 0_6 & 0_6 \\ 0_6 & 0_6 & A_1 & 0_6 & 0_6 & I_6 & 0_6 \\ 0_6 & 0_6 & 0_6 & A_1 & 0_6 & 0_6 & I_6 \\ \hline 0_6 & 3n_o^2 I_6 & 0_6 & 0_6 & A_1 & 2n_o I_6 & 0_6 \\ 0_6 & 0_6 & 0_6 & 0_6 & -2n_o I_6 & A_1 & 0_6 \\ \hline 0_6 & 0_6 & 0_6 & -n_o^2 I_6 & 0_6 & 0_6 & A_1 \end{array}\right] \tag{27}$$

$$\text{where} \quad A_1 = \left[\begin{array}{ccc|ccc} 0 & 0 & 0 & 1 & 0 & 0 \\ 0 & 0 & 0 & 0 & 1 & 0 \\ 0 & 0 & 0 & 0 & 0 & 1 \\ \hline 3n_o^2 & 0 & 0 & 0 & 2n_o & 0 \\ 0 & 0 & 0 & -2n_o & 0 & 0 \\ 0 & 0 & -n_o^2 & 0 & 0 & 0 \end{array}\right] , \quad M_i = \frac{3}{2}\frac{n_o^2}{\bar{R}_o}\left[\begin{array}{c|c} 0_3 & 0_3 \\ \hline M_i' & 0_3 \end{array}\right] , \quad M_1' = \begin{bmatrix} -2 & 0 & 0 \\ 0 & 1 & 0 \\ 0 & 0 & 1 \end{bmatrix}, \; M_2' = \begin{bmatrix} 0 & 1 & 0 \\ 1 & 0 & 0 \\ 0 & 0 & 0 \end{bmatrix}, \; M_3' = \begin{bmatrix} 0 & 0 & 1 \\ 0 & 0 & 0 \\ 1 & 0 & 0 \end{bmatrix}$$

Position response due to initial condition excitation is given by the expression

$$y(t) = h_0(t) = \bar{C}(t)\bar{\Phi}(t,0)x_0^{\otimes}$$
$$\text{where} \quad \bar{\Phi}(t,0) = e^{\int_0^t \bar{A}(\tau)d\tau} \quad , \quad y = [x \;\; y \; z]^T \tag{28}$$

Computation of the state transition matrix $\bar{\Phi}$ is required. The approach taken is based on Laplace transform inversion of the resolvent matrix, which requires analytical inversion of matrix $(sI-\bar{A})$ where "s" denotes complex frequency. This task is the most computationally intensive step of the entire solution. Typically, a complete symbolic state transition solution is not feasible when dynamic order is larger than four, since symbolic polynomial factoring is not possible beyond the quartic degree. However, recall the CW model has dynamic order six with two roots at 0 and four roots at $\pm in_o$ and allows a complete solution due to matrix sparseness and polynomial symmetry. The quadratic Volterra (QV) model is similarly sparse and symmetric, and has numerically obtained roots 0 (fourteen), $\pm in_o$ (twenty), $\pm i2n_o$ (eight). With these observations, complete solution existence was postulated. Using both symbolic computational software and manual calculations, a successful completion to the calculation was achieved. Ample use of the partitioned matrix inverse formula was made [22]. After transforming back to the time domain, pre-multiplying by the output matrix, and post-multiplying by the initial condition vector, expressions for the initial condition response of deputy relative position, which is identical to the 0^{th} order Volterra kernel under the stated assumptions, are available. These expressions, which are accurate to second order, are given in Eq. (29). In these equations, subscript "0" denotes the value of a quantity at the initial time, and "t" represents time elapsed since the initial time.

$$
\begin{aligned}
& x(t) \\
= \;& \{4-3C_{n_ot}\}x_0 \\
+ \;& \{\tfrac{1}{n_o}S_{n_ot}\}\dot{x}_0 + \{\tfrac{2}{n_o}(1-C_{n_ot})\}\dot{y}_0 \\
+ \;& \{\tfrac{3}{2}\tfrac{1}{\bar{R}_o}(7-10C_{n_ot}+3C_{2n_ot}+12n_otS_{n_ot}-12n_o^2t^2)\}x_0^2 \\
+ \;& \{\tfrac{3}{2}\tfrac{1}{\bar{R}_o}(1-C_{n_ot})\}y_0^2 \\
+ \;& \{\tfrac{1}{4}\tfrac{1}{\bar{R}_o}(3-2C_{n_ot}-C_{2n_ot})\}z_0^2 \\
+ \;& \{\tfrac{1}{2}\tfrac{1}{n_o^2\bar{R}_o}(-3+4C_{n_ot}-C_{2n_ot})\}\dot{x}_0^2 \\
+ \;& \{\tfrac{1}{2}\tfrac{1}{n_o^2\bar{R}_o}(6-10C_{n_ot}+4C_{2n_ot}+12n_otS_{n_ot}-9n_o^2t^2)\}\dot{y}_0^2 \\
+ \;& \{\tfrac{1}{4}\tfrac{1}{n_o^2\bar{R}_o}(3-4C_{n_ot}+C_{2n_ot})\}\dot{z}_0^2 \\
+ \;& 2\{3\tfrac{1}{\bar{R}_o}(-S_{n_ot}+n_ot)\}x_0y_0 \\
+ \;& 2\{\tfrac{3}{2}\tfrac{1}{n_o\bar{R}_o}(4S_{n_ot}-S_{2n_ot}-4n_ot+2n_otC_{n_ot})\}x_0\dot{x}_0 \\
+ \;& 2\{\tfrac{3}{2}\tfrac{1}{n_o\bar{R}_o}(4-6C_{n_ot}+2C_{2n_ot}+7n_otS_{n_ot}-6n_o^2t^2)\}x_0\dot{y}_0 \\
+ \;& 2\{\tfrac{3}{2}\tfrac{1}{n_o\bar{R}_o}(-S_{n_ot}+n_ot)\}y_0\dot{y}_0 \\
+ \;& 2\{\tfrac{1}{4}\tfrac{1}{n_o\bar{R}_o}(2S_{n_ot}-S_{2n_ot})\}z_0\dot{z}_0 \\
+ \;& 2\{\tfrac{1}{2}\tfrac{1}{n_o^2\bar{R}_o}(7S_{n_ot}-2S_{2n_ot}-6n_ot+3n_otC_{n_ot})\}\dot{x}_0\dot{y}_0
\end{aligned}
$$

$$
\begin{aligned}
& y(t) \\
= \;& \{6(S_{n_ot}-n_ot)\}x_0 + \{1\}y_0 \\
+ \;& \{\tfrac{2}{n_o}(-1+C_{n_ot})\}\dot{x}_0 + \{\tfrac{1}{n_o}(4S_{n_ot}-3n_ot)\}\dot{y}_0 \\
+ \;& \{\tfrac{3}{4}\tfrac{1}{\bar{R}_o}(40S_{n_ot}+3S_{2n_ot}-22n_ot-24n_otC_{n_ot})\}x_0^2 \\
+ \;& \{3\tfrac{1}{\bar{R}_o}(S_{n_ot}-n_ot)\}y_0^2 \\
+ \;& \{\tfrac{1}{4}\tfrac{1}{\bar{R}_o}(4S_{n_ot}+S_{2n_ot}-6n_ot)\}z_0^2 \\
+ \;& \{\tfrac{1}{4}\tfrac{1}{n_o^2\bar{R}_o}(8S_{n_ot}-S_{2n_ot}-6n_ot)\}\dot{x}_0^2 \\
+ \;& \{\tfrac{1}{n_o^2\bar{R}_o}(10S_{n_ot}+S_{2n_ot}-6n_ot-6n_otC_{n_ot})\}\dot{y}_0^2 \\
+ \;& \{\tfrac{1}{4}\tfrac{1}{n_o^2\bar{R}_o}(8S_{n_ot}-S_{2n_ot}-6n_ot)\}\dot{z}_0^2 \\
+ \;& 2\{\tfrac{3}{2}\tfrac{1}{\bar{R}_o}(1-C_{n_ot})\}x_0y_0 \\
+ \;& 2\{\tfrac{3}{4}\tfrac{1}{n_o\bar{R}_o}(-5+4C_{n_ot}+C_{2n_ot}+4n_otS_{n_ot})\}x_0\dot{x}_0 \\
+ \;& 2\{\tfrac{3}{2}\tfrac{1}{n_o\bar{R}_o}(12S_{n_ot}+S_{2n_ot}-7n_ot-7n_otC_{n_ot})\}x_0\dot{y}_0 \\
+ \;& 2\{\tfrac{3}{2}\tfrac{1}{n_o\bar{R}_o}(-S_{n_ot}+n_ot)\}y_0\dot{x}_0 \\
+ \;& 2\{\tfrac{1}{4}\tfrac{1}{n_o\bar{R}_o}(-3+4C_{n_ot}-C_{2n_ot})\}z_0\dot{z}_0 \\
+ \;& 2\{\tfrac{1}{2}\tfrac{1}{n_o^2\bar{R}_o}(-3+2C_{n_ot}+C_{2n_ot}+3n_otS_{n_ot})\}\dot{x}_0\dot{y}_0
\end{aligned}
$$

(29)

$$
\begin{aligned}
& z(t) \\
= \;& \{C_{n_ot}\}z_0 + \{\tfrac{1}{n_o}S_{n_ot}\}\dot{z}_0 \\
+ \;& 2\{\tfrac{3}{4}\tfrac{1}{\bar{R}_o}(-3+2C_{n_ot}+C_{2n_ot}+4n_otS_{n_ot})\}x_0z_0 \\
+ \;& 2\{\tfrac{3}{4}\tfrac{1}{n_o\bar{R}_o}(2S_{n_ot}+S_{2n_ot}-4n_otC_{n_ot})\}x_0\dot{z}_0 \\
+ \;& 2\{\tfrac{1}{4}\tfrac{1}{n_o\bar{R}_o}(2S_{n_ot}-S_{2n_ot})\}z_0\dot{x}_0 \\
+ \;& 2\{\tfrac{1}{2}\tfrac{1}{n_o\bar{R}_o}(-3+2C_{n_ot}+C_{2n_ot}+3n_otS_{n_ot})\}z_0\dot{y}_0 \\
+ \;& 2\{\tfrac{1}{4}\tfrac{1}{n_o^2\bar{R}_o}(3-4C_{n_ot}+C_{2n_ot})\}\dot{x}_0\dot{z}_0 \\
+ \;& 2\{\tfrac{1}{2}\tfrac{1}{n_o^2\bar{R}_o}(S_{n_ot}+S_{2n_ot}-3n_otC_{n_ot})\}\dot{y}_0\dot{z}_0
\end{aligned}
$$

Equation (29) indicates time dependent deputy positions are nonlinear functions of the initial position and velocity; specifically linear, quadratic, and bilinear combinations of x_0, y_0, z_0, $\dot{x}_0$, $\dot{y}_0$, $\dot{z}_0$. All combinations of terms are present in at least one of the expressions except for terms y_0z_0 and $y_0\dot{z}_0$, which are absent. Note the linear terms x_0, y_0, z_0, $\dot{x}_0$, $\dot{y}_0$, $\dot{z}_0$ are precisely the CW solution. Modeling of quadratic gravitational nonlinearities have introduced new secular terms not found in the linear CW solution including $n_o t\cos(n_o t)$, $n_o t\sin(n_o t)$, and $(n_o t)^2$. Secular terms in x include $n_o t$, $n_o t\cos(n_o t)$, $n_o t\sin(n_o t)$, $(n_o t)^2$, while secular terms in y include only $n_o t$, $n_o t\cos(n_o t)$, $n_o t\sin(n_o t)$, and secular terms in z are limited to just $n_o t\cos(n_o t)$, $n_o t\sin(n_o t)$. While the linear CW solution experiences drift in only the transverse (y) axis, the nonlinear QV solution also captures motion drift in the radial (x) and normal (z) axes. The new solution permits alteration of the in-track drift rate through extra terms not present in the CW solution. While these secular terms reflect the local three-dimensional departure of the deputy away from the chief over time, they eventually will fail in predicting the true globally bounded relative motion, as they are a class of perturbation solutions with a limited temporal window. Although the second order solution might provide higher accuracy than the first order solution for a given separation distance between chief and deputy, the second order solution may diverge more rapidly than the first order solution as that separation gets larger. Quadratic gravitational nonlinearities have also resulted in the possibility of bias offset in the cross-track z behavior, as well as a new frequency at $2n_o$ in all axes. As a final observation, the QV solution allows bidirectional coupling between the radial/in-track in-plane motion and the cross-track out-of-plane motion; a mechanism present in the full nonlinear differential equations but absent in the CW linear differential equations and solution.

5. Numeric Example

To test and validate accuracy of the new relative motion solution, a numerical example with two cases is offered. Conditions for the Case A example originally appeared in Ref. [15]. Case B is obtained by uniform ten-fold scaling of the Case A deputy initial conditions. Circular chief orbital elements and deputy relative initial conditions for both cases are specified in Eq. (30) below. Three responses are generated for each case. The first response is nonlinear simulation based on Eq. (14) using Runge-Kutta 4th order numerical integration. This result is taken as the "exact" solution. The second response is the closed-form CW linear solution. The third response is the new closed-form QV nonlinear solution given in Eq. (29). Simulation parameters include $\mu = 398{,}600\ \text{km}^3/\text{s}^2$, $R_E = 6{,}378$ km, and time step $\Delta t = (2\pi/n_o)/3600$ (0.1 deg latitude steps) with rad/s units for n_o.

$$
\begin{array}{ll}
 & \text{Deputy - Case A:} \\
\text{Chief:} & x_0 = -0.000288947081\ \text{km}\ ,\ \dot{x}_0 = 0.000263388377\ \text{km/s} \\
\bar{R}_o = 7100\ \text{km} & y_0 = 0.50033326318\ \ \text{km}\ ,\ \dot{y}_0 = 0.000000272412\ \text{km/s} \\
\bar{\Omega}_o = 45\ \ \text{deg} & z_0 = 0.000175666681\ \text{km}\ ,\ \dot{z}_0 = 0.000527371445\ \text{km/s} \\
\bar{i}_o = 70\ \ \text{deg} & \text{Deputy - Case B:} \\
\bar{\theta}_o = 0\ \ \text{deg} & x_0 = -0.00288947081\ \text{km}\ ,\ \dot{x}_0 = 0.00263388377\ \text{km/s} \\
 & y_0 = 5.0033326318\ \ \text{km}\ ,\ \dot{y}_0 = 0.00000272412\ \text{km/s} \\
 & z_0 = 0.00175666681\ \text{km}\ ,\ \dot{z}_0 = 0.00527371445\ \text{km/s}
\end{array}
\qquad (30)
$$

Figures 2-4 show the Case A CW and QV error relative to nonlinear simulation (NLS) for the x, y, z axes; that is, at each time step the value of the quantity predicted by CW or QV is subtracted from the predicted NLS solution. The QV solution is significantly more accurate than the CW solution for this case. Although the CW solution error in the x and z axes is not very large for this approximately 0.5 km relative orbit, the QV solution error is much less. The most significant improvement occurs in the y axis. After 15 chief orbits, the error in the QV in-track solution is several orders of magnitude less than the CW solution (0.0004 vs. 11.2 m). New terms in Eq. (29), arising from inclusion of quadratic gravitational effects, facilitate better prediction of the in-track drift, a common deficiency of the CW technique. Figure 5 shows the overlay plot of the in-track responses near the maximum values on the 14^{th} orbit. The CW propagated deputy experiences a peak in-track departure of approximately 10 m from the NLS propagated deputy, while for the resolution shown in this plot, the QV propagated deputy appears to lie on top of the NLS deputy at this same instant. Figures 6-7 show the orbital tracks over the 15 orbit prediction where the deputy relative orbit is advancing further ahead of the chief. Progression of error growth in the CW solution is clearly seen with each successive orbit, while the QV solution maintains accuracy to the sub-meter level.

Figures 8-10 show the Case B CW and QV relative errors in all axes. The Volterra solution response is again significantly more accurate than the CW solution for this approximately 5 km relative orbit. In the x and z axes, the CW errors are on the order of 10 m while the QV error is near 1 m. Improvement in the y axis is again the most significant. After 15 chief orbits, the Volterra in-track solution maintains several orders of magnitude improvement (0.39 vs. 1,120 m). Figures 11-12 shows the overlay plots of the in-track responses overall and near the maximum values on the 14^{th} orbit. Observe in Fig. 11 the in-track drift for the CW and QV-NLS solutions are in different directions. This feature is more easily observed in the orbital track plot in Fig. 13. The CW deputy relative orbit is advancing ahead of the chief as in the first case, while the QV and NLS orbits are retreating back towards the chief. The CW drift rate scales linearly with the initial conditions, while the QV drift rate scales differently through the additional nonlinear initial condition terms in Eq. (29). The second order analytic solution is sufficiently versatile to reflect this nonlinear behavior.

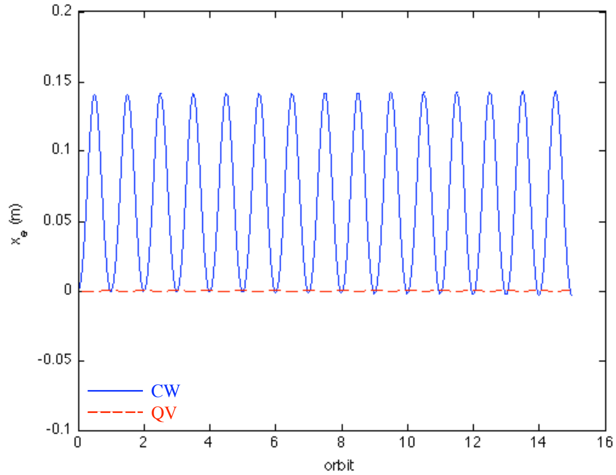

Figure 2. x Error for Case A

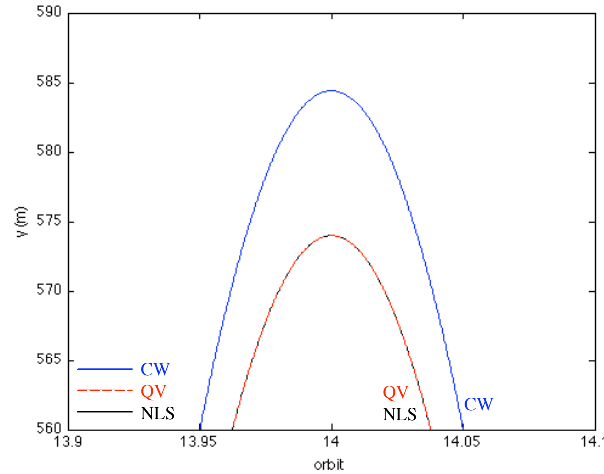

Figure 5. y Absolute for Case A, Enlarged

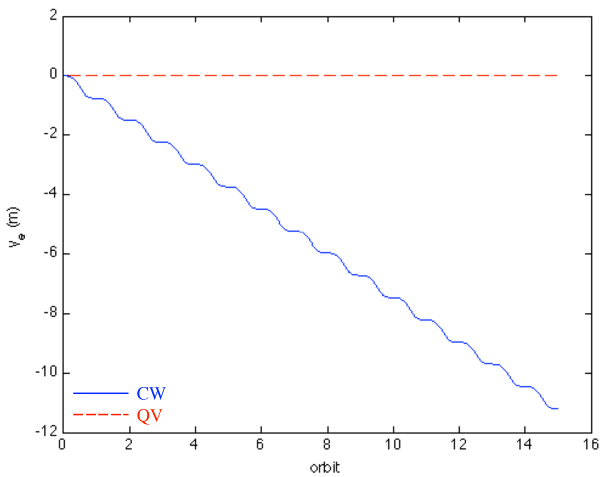

Figure 3. y Error for Case A

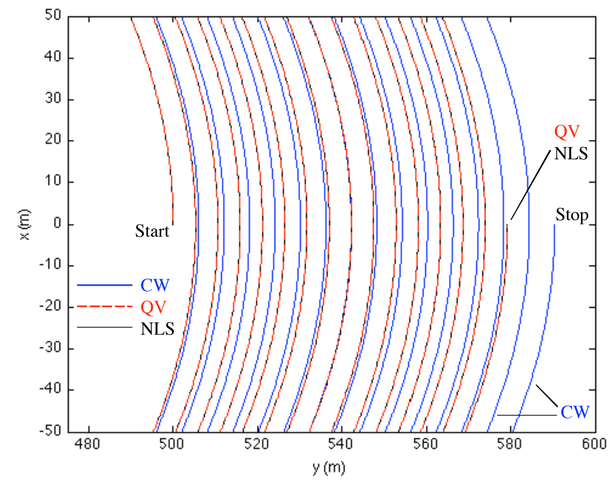

Figure 6. x,y Absolute for Case A

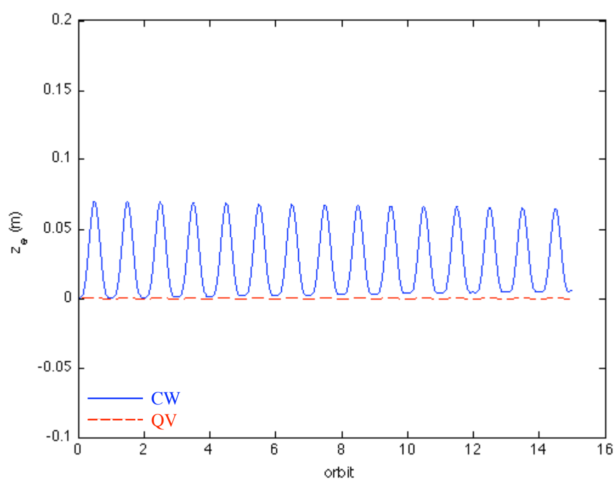

Figure 4. z Error for Case A

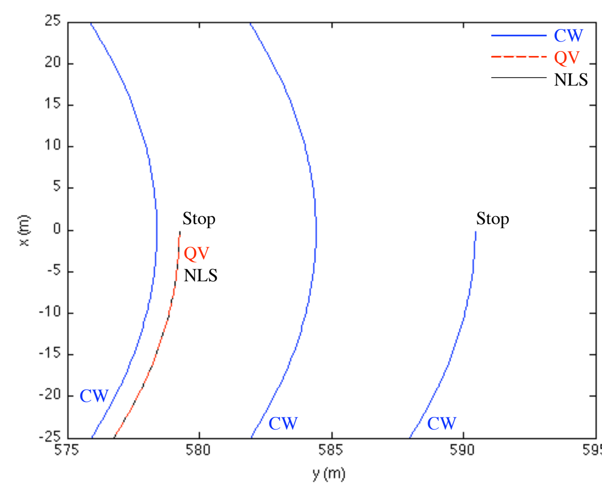

Figure 7. x,y Absolute for Case A, Enlarged

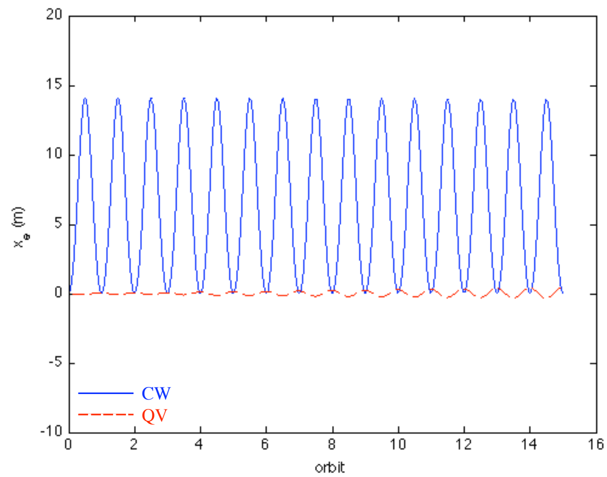

Figure 8. x Error for Case B

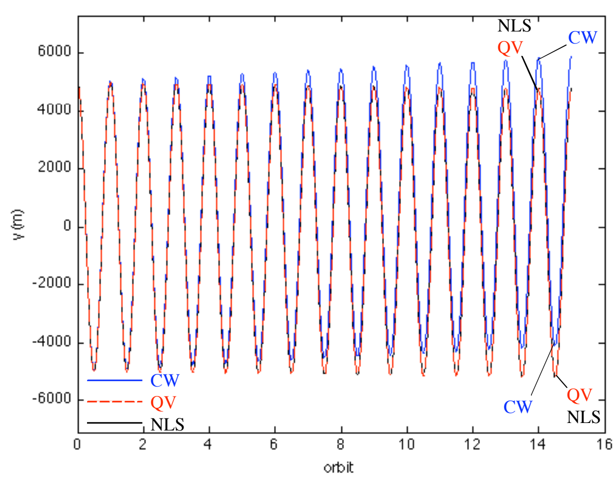

Figure 11. y Absolute for Case B

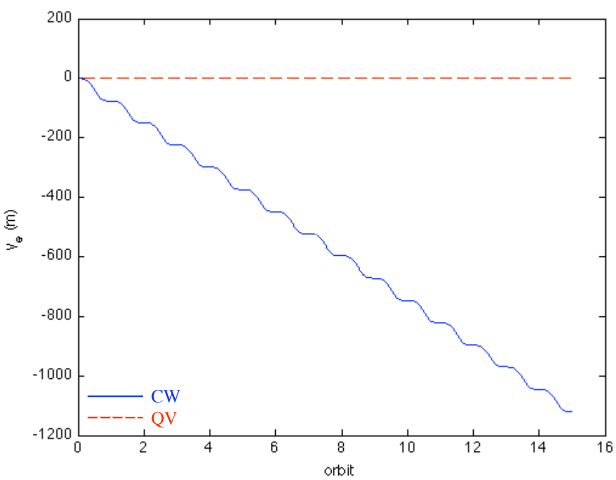

Figure 9. y Error for Case B

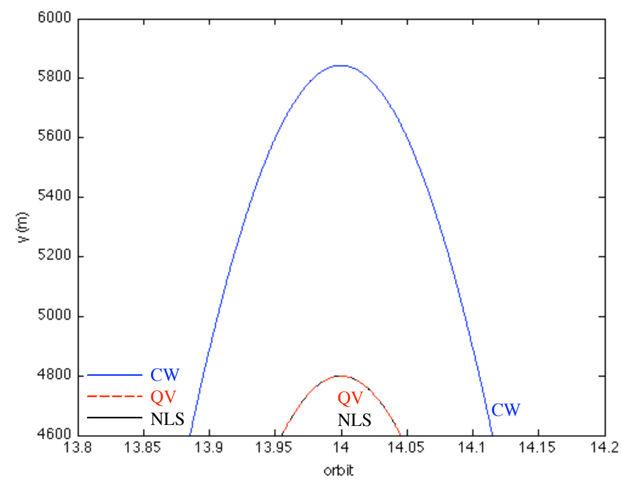

Figure 12. y Absolute for Case B, Enlarged

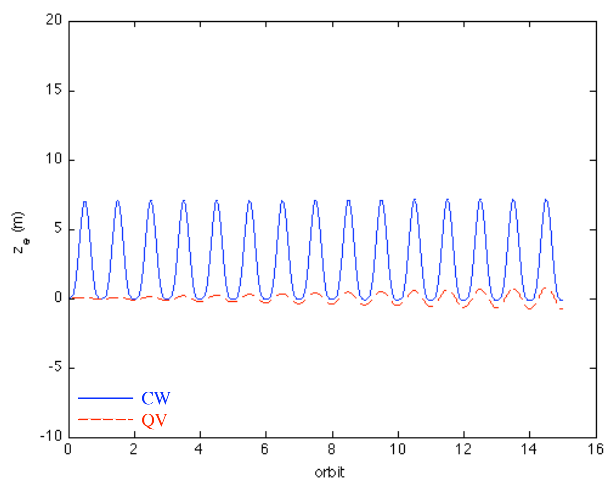

Figure 10. z Error for Case B

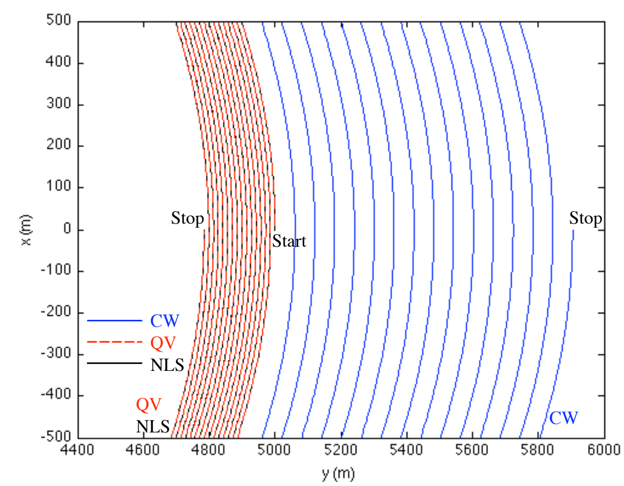

Figure 13. x,y Absolute for Case B

6. Nonlinear Revelation

Improved accuracy from the quadratic Volterra solution is one important aspect of the new results. Another important aspect concerns the analytic nature of the solution, and what it can reveal regarding physical mechanisms within nonlinear relative orbital motion. Consider collecting all initial conditions multiplying secular term $n_o t$ in the in-track expression in Eq. (29), or

$$y(t) = \ldots + \{-6x_0 - \frac{3}{n_o}\dot{y}_0 - \frac{3}{2}\frac{1}{\bar{R}_o}(11x_0^2+2y_0^2+z_0^2) - \frac{3}{2}\frac{1}{n_o^2\bar{R}_o}(\dot{x}_0^2+4\dot{y}_0^2+\dot{z}_0^2) + \frac{3}{n_o\bar{R}_o}(-7x_0\dot{y}_0+y_0\dot{x}_0)\}n_o t + \ldots \tag{31}$$

These initial conditions can be grouped according to whether they are linear in the states (c_l), quadratic in position (c_{qp}), quadratic in rate (c_{qr}), or bilinear in position and rate (c_{bpr}). Table 1 summarizes these various groups, including the total group of terms as well (c_t). Considerable insight can be extracted from these expressions. The nonlinear terms are proportional to $1/\bar{R}_o$, $1/(n_o^2\bar{R}_o)$, and $1/(n_o\bar{R}_o)$. For small orbits (quantified by small initial positions and rates), the linear terms will dominate the in-track drift rate. For larger orbits, the significance of the nonlinear terms can increase to the point where they influence the in-track drift rate, or even dominate it. For example, by equating the contribution from x_0 and x_0^2, the condition for which one term dominates over the other can be assessed in a very simple way. The contributions of the two terms are balanced when the initial radial position is four elevenths of the chief radius, or

$$6x_0 = \frac{3}{2}\frac{1}{\bar{R}_o}11x_0^2 \quad \rightarrow \quad x_0 = \frac{4}{11}\bar{R}_o \tag{32}$$

The complete set of coefficient expressions not only reveal the different scalings between linear and nonlinear terms, but also between the various types of nonlinear terms. For example, in reference to the c_{qp} term, the x_0^2 contribution to drift rate is 5.5 times stronger than the y_0^2 contribution and 11 times stronger than the z_0^2 contribution.

Table 1. Initial Condition Groups for y Axis Secular Term

Group	Term
c_t	$-6x_0 - \frac{3}{n_o}\dot{y}_0 - \frac{3}{2}\frac{1}{\bar{R}_o}(11x_0^2+2y_0^2+z_0^2) - \frac{3}{2}\frac{1}{n_o^2\bar{R}_o}(\dot{x}_0^2+4\dot{y}_0^2+\dot{z}_0^2) + \frac{3}{n_o\bar{R}_o}(-7x_0\dot{y}_0+y_0\dot{x}_0)$
c_l	$-6x_0 - \frac{3}{n_o}\dot{y}_0$
c_{qp}	$-\frac{3}{2}\frac{1}{\bar{R}_o}(11x_0^2+2y_0^2+z_0^2)$
c_{qr}	$-\frac{3}{2}\frac{1}{n_o^2\bar{R}_o}(\dot{x}_0^2+4\dot{y}_0^2+\dot{z}_0^2)$
c_{bpr}	$+\frac{3}{n_o\bar{R}_o}(-7x_0\dot{y}_0+y_0\dot{x}_0)$

Table 2 lists numeric values for these coefficient groups for the two cases. The c_t group representing all terms changes sign between the two cases (positive for Case A with advancing drift, negative for Case B with retreating drift), while the c_l group representing only the linear terms is positive for both cases. After examining the other coefficients, note the quadratic rate and bilinear position-rate terms approximately cancel one another leaving the quadratic position terms as the primary cause of the in-track drift rate reversal. It would be very difficult, or tedious, to uncover such insights from nonlinear simulation alone. Independent verification of these conclusions can be achieved in this simple example from two-body motion theory. Table 3 lists the chief and deputy semi-major axis (a) and specific energy ($\mathcal{E}$) for the two cases. For Case A, the deputy has a smaller semi-major axis and lower energy level compared with the chief, while in Case B, the deputy has a larger semi-major axis and higher energy level than for the chief. This difference in semi-major axis or energy level is the root cause of the nonlinear in-track drift reversal. For Case B, the deputy is orbiting Earth at a higher radius, and hence at a lower velocity, when compared to the chief, and thus relative drift is retrograde. The opposite conditions happen in Case A leading to direct relative drift.

Table 2. Initial Condition Group Data

Group	Case A	Case B
c_t (km)	+0.0008404449877904054	-0.002290761101582208
c_l (km)	+0.0009592806653402528	+0.009592806653402529
c_{qp} (km)	-0.0001056480853754877	-0.01056480853754877
c_{qr} (km)	-0.00006592018856900161	-0.006592018856900161
c_{bpr} (km)	+0.00005273259639464191	+0.005273259639464191

Table 3. Vehicle Semi-Major Axis and Specific Energy Data

Vehicle	a (km)	$\mathcal{E}$ (km^2/s^2)
Chief	7100	-28.07042253521128
Deputy - Case A	7099.999439703345	-28.07042475038945
Deputy - Case B	7100.001527173064	-28.07041649741071

7. Conclusions

Application of Volterra series theory with support from Carleman linearization has been successfully applied to space vehicle relative motion, under certain assumptions. A complete second order framework from differential equation set to its closed-form response solution is offered. The solution is a generalization of the widely used linear Clohessy-Wiltshire solution for relative motion and significantly improves on the propagated motion accuracy. The analytic nature of the solution offers a new insightful window besides nonlinear simulation for investigating phenomena such as in-track drift strength and direction changes, radial and cross-track drift mechanisms, cross-track bias offsets, higher harmonic motions, and in-plane/out-of-plane coupling. This area of study appears to be rich for further investigative efforts. In addition, future work in this area will include deriving a Volterra solution incorporating J_2 gravity perturbation.

8. References

[1] Hill, G. W., "Researches in the Lunar Theory," American Journal of Mathematics, Vol. 1, No. 1, March, 1878, pp. 5-26.

[2] Clohessy, W. H. and Wiltshire, R. S., "Terminal Guidance System for Satellite Rendezvous," Journal of the Aerospace Sciences, Vol. 27, No. 9, September, 1960, pp. 653-658.

[3] Lawden, D. F., "Optimal Trajectories for Space Navigation," Butterworth, London, England, 1963.

[4] Tschauner, J. and Hempel, P., "Rendezvous with a Target in Elliptic Orbit," Astronautica Acta, Vol. 11, No. 2, March-April, 1965, pp. 104-109.

[5] Carter, T. E., "New Form for the Optimal Rendezvous Equations Near Keplerian Orbit," Journal of Guidance, Control, and Dynamics, Vol. 13, No. 1, January-February, 1990, pp. 183-186.

[6] Carter, T. E., "State Transition Matrices for Terminal Rendezvous Studies: Brief Survey and New Example," Journal of Guidance, Control, and Dynamics, Vol. 21, No. 1, January-February, 1998, pp. 148-155.

[7] Yamanaka, K. and Ankersen, F., "New State Transition Matrix for Relative Motion on an Arbitrary Elliptical Orbit," Journal of Guidance, Control, and Dynamics, Vol. 25, No. 1, January-February, 2002, pp. 60-66.

[8] Inalhan, G., Tillerson, M., and How, J. P., "Relative Dynamics and Control of Spacecraft Formations in Eccentric Orbits," Journal of Guidance, Control, and Dynamics, Vol. 25, No. 1, January-February, 2002, pp. 48-59.

[9] Hablani, H. B., Tapper, M. L., and Dana-Bashian, D. J., "Guidance and Relative Navigation for Autonomous Rendezvous in a Circular Orbit," Journal of Guidance, Control, and Dynamics, Vol. 25, No. 3, May-June, 2002, pp. 553-562.

[10] Okasha, M. and Newman, B., "Relative Motion and Autonomous Rendezvous in Keplerian Elliptic Orbits," AIAA-2010-7593, Proceedings of the AIAA Guidance, Navigation, and Control Conference, Toronto, Ontario, Canada, August, 2010.

[11] Schweighart, S. A. and Sedwick, R. J., "High-Fidelity Linearized J_2 Model for Satellite Formation Flight," Journal of Guidance, Control, and Dynamics, Vol. 25, No. 6, November-December, 2002, pp. 1073-1080.

[12] Ross, I. M., "Linearized Dynamic Equations for Spacecraft Subject to J_2 Perturbation," Journal of Guidance, Control, and Dynamics, Vol. 26, No. 4, July-August, 2003, pp. 657-659.

[13] Sengupta, P., Vadali, S. R., and Alfriend, K. T., "Averaged Relative Motion and Applications to Formation Flight Near Perturbed Orbits," Journal of Guidance, Control, and Dynamics, Vol. 31, No. 2, March-April, 2008, pp. 258-272.

[14] Gim, D. W. and Alfriend, K. T., "State Transition Matrix of Relative Motion for the Perturbed Noncircular Reference Orbit," Journal of Guidance, Control, and Dynamics, Vol. 26, No. 6, November-December, 2003, pp. 956-971.

[15] Vadali, S., "Model for Linearized Satellite Relative Motion About a J_2-Perturbed Mean Circular Orbit," Journal of Guidance, Control, and Dynamics, Vol. 32, No. 5, September-October 2009, pp. 1687-1691.

[16] Vaddi, S. S., Vadali, S. R., and Alfriend, K. T., "Formation Flying: Accommodating Nonlinearity and Eccentricity Perturbations," Journal of Guidance, Control, and Dynamics, Vol. 26, No. 2, March-April, 2003, pp. 214-223.

[17] Condurache, D. and Martinusi, V., "Kepler's Problem in Rotating Reference Frames Part 2: Relative Orbital Motion," Journal of Guidance, Control, and Dynamics, Vol. 30, No. 1, January-February, 2007, pp. 201-213.

[18] Condurache, D. and Martinusi, V., "Quaternionic Exact Solution to the Relative Orbital Motion Problem," Journal of Guidance, Control, and Dynamics, Vol. 33, No. 4, July-August, 2010, pp. 1035-1047.

[19] Omran, A. and Newman, B., "Nonlinear Analytical Solution of Relative Motion Subject to J_2 Perturbation Using Volterra Kernels," AAS-2011-467, Proceedings of the AAS-AIAA Astrodynamics Specialist Conference, Girdwood, Alaska, July-August, 2011, Advances in the Astronautical Sciences, Vol. 142, pp. 987-1006.

[20] Volterra, V., "Theory of Functionals and of Integral and Integro-Differential Equations," Dover, New York, New York, 1958.

[21] Rugh, W., "Nonlinear System Theory: The Volterra/Wiener Approach," Johns Hopkins University Press, Baltimore, Maryland, 1981.

[22] Noble, B. and Daniel, J. W., "Applied Linear Algebra," Prentice-Hall, Englewood Cliffs, New Jersey, 1977.